Front formation in an active scalar equation

Peter Constantin and Qing Nie
Department of Mathematics, The University of Chicago, 5734 South University Avenue, Chicago, Illinois 60637

Norbert Schörghofer
James Franck Institute, The University of Chicago, 5640 South Ellis Avenue, Chicago, Illinois 60637

(Received 21 December 1998)

We study the formation of thermal fronts in an active scalar equation that is similar to the Euler equation. For a particular initial condition, an earlier candidate for finite-time blowup, the front forms in a generalized self-similar way with constant hyperbolicity at the center. The behavior belongs to a class of scenarios for which finite-time blowup is impossible. A systematic exploration of many different initial conditions reveals no evidence of singular solutions. [S1063-651X(99)10107-7]

PACS number(s): 47.10.+g, 02.60.−x

I. INTRODUCTION

There are numerous active scalar equations in fluid dynamics; perhaps none is more familiar than the two-dimensional Euler equation for an incompressible fluid: $\partial\omega/\partial t+\mathbf{v}\cdot\nabla\omega=0$. The vorticity $\omega=\nabla\times\mathbf{v}$ is advected and at the same time determines the velocity field. Another, geophysically relevant, example is provided by the surface behavior of quasigeostrophic flow with uniform interior potential vorticity on a flat bottom [1,2]. Adiabatic temperature variations cause pressure fields that drive winds and at the same time are transported by the wind. The motion of the temperature contour lines is similar to the motion of vortex lines in the three-dimensional (3D) Euler equation, but opens the possibility of finite-time singularities even in two dimensions [3]. The steepening of temperature fronts in surface quasigeostrophic flow (SQG) is the topic of this paper. For the study of singularities of convection equations, Dombret *et al.* [4] also considered the problem of convection in two-dimensional porous media that is similar to SQG in scaling but is not isotropic. They reported a strong gradient growth of the solution, however, the equation might not display the strong geometric depletion of nonlinearity present in the Euler equation and SQG.

The active scalar of surface quasigeostrophic flow is given by an advection equation for the (potential) temperature θ,

$$\frac{\partial\theta}{\partial t}+\mathbf{v}\cdot\nabla\theta=0, \tag{1}$$

where the velocity is determined by θ at each time, but is a nonlocal function of it [1,2,5].

$$v(r)=\int\frac{\nabla^{\perp}\theta(r')}{|r-r'|}dr'\Leftrightarrow\hat{v}(k)=i\frac{k^{\perp}}{|k|}\hat{\theta}(k). \tag{2}$$

The symbol $\nabla^{\perp}$ refers to a vector perpendicular to the gradient, that is, along a contour line. $r=(x,y)$ is a two-dimensional vector. Since v is a convolution integral it can be obtained locally in Fourier variables.

The velocity in the incompressible Euler equation is given by a rather similar expression $\hat{v}(k)=ik\times\hat{\omega}/k^2$, only different by the power of k in the denominator. The vorticity $\omega=\nabla\times\mathbf{v}$ in the 2D Euler equation also obeys an advection equation and in 3D evolves according to the same equation as the contour lines of the active scalar $\nabla^{\perp}\theta$ [3,6]. This analogy between the two-dimensional SQG equation and the Euler equation serves as motivation to study singularity formation in SQG. Independent of this motivation, SQG describes the temperature field in rapidly rotating stratified fluids, like large thermal fronts in planetary atmospheres and oceans.

The organization of the paper is as follows. In Sec. II we discuss evidence for the absence of a finite-time singularity for SQG using initial condition (3). Besides this major conclusion drawn earlier [7], the numerical solutions are used to make several further observations. The local scenario of the front steepening is investigated in Sec. III and more general initial conditions are explored in Sec. IV.

II. ABSENCE OF FINITE-TIME SINGULARITY

As suggested in [8,3], the commonly used initial condition for studying SQG is

$$\theta(x,y;0)=\sin(x)\sin(y)+\cos(y). \tag{3}$$

All studies in this section and the next use this initial condition. The first numerical simulations of SQG to study the possible singularity formation [8] obtained an empirical asymptotic fit $\max|\nabla\theta|\sim 1/(8.25-t)^{1.7}$, consistent with finite-time blowup. The work [9] argues that the asymptotic behavior can equally well be fitted with a double exponential $\exp\{\exp[b(t-t_0)]\}$, ruling out a finite-time blowup. No fitted values for b and t_0 have been reported. Although these two forms can be very close to each other over a certain interval of time, the mathematical implications of the two fits are tremendously different: one fit predicts a finite-time blowup and the other does not. The blowup scenario of [3] was investigated rigorously by Cordoba [10], who proved that it cannot lead to finite-time blowup. Recently [7], we showed numerically that the maximum gradient grows at most

TABLE I. Chronologically ordered list of numerical results for initial condition (3).

Year	Asymptotic form of maximum gradient	Max. resolution	Reference
1994	$\max\|\nabla\theta\|=c/(8.25-t)^{1.7}$	1024^2	[8,3]
1997	$\max\|\nabla\theta\|=\exp\{\exp[b(t-t_0)]\}$	2048^2	[9]
1998	$\max\|\nabla\theta\|\leqslant\exp\{\exp[0.38(t-4.1)]\}$	4096^2	[7]

double exponentially fast, and obtained b and t_0 numerically. The three major numerical results on this subject are summarized in Table I.

The major issues for estimating the asymptotic behavior of the solution numerically are the checking of the resolution and the study of suitable quantities: some of them are more prone to numerical errors than others. We use two numerical methods (pseudospectral and fourth order [11]) to solve the equation. The two methods have different spatial smoothing and different cutoffs of high modes. For time stepping the fourth order Runge-Kutta scheme has been applied, since its linear time step requirement is superior to other standard explicit time stepping schemes [12,11]. The velocity field is obtained in Fourier space.

There are several parameters in the scheme that should not influence the result: spatial resolution, temporal resolution, and the parameters in the artificial damping. For example, Fig. 1 shows a convergence test for the spatial errors in the maximum gradient of θ for different grid resolutions. The result appears accurate up to $t\approx 6.4$ and under-resolving would lead, in the short run, to an exaggerated gradient. Similar convergence or independence tests for the gradient (and the stretch rate) have been carried out with the size of the time step and the parameters for the artificial damping of both methods. References [7,11] contain further details on the numerics.

Figure 2 demonstrates the rapid growth of the maximum gradient. The dots are the stretch rate of the contour lines, which is the logarithmic derivative of the maximum gradient, and it can be equivalently considered as a blowup criterion. The stretch rate can be independently computed from the velocity field together with the first and second derivatives of θ [3]. Agreement of the two provides another demanding numerical test.

The stretch rate in Fig. 2 shows no tendency to blowup [7]. Even without the final dip in the curve the stretch rate is bounded by an exponential. This is determined using two numerical methods with two independent ways of measuring the stresses and all four measurements agree with each other and converge with grid resolution and with the other parameters of the numerical scheme. The exponential bound leads to a maximum gradient that grows at most like a double exponential [13] and, therefore, no finite-time singularity.

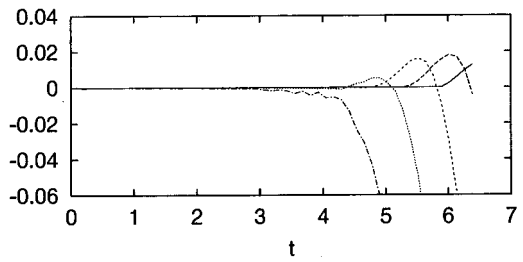

FIG. 1. Relative differences in maximum gradient measurements for different resolutions. The resolutions 128^2, 256^2, 512^2, 1024^2, and 2048^2 are compared with the highest resolution run of 4096^2. They have all been done with the fourth order method.

III. SELF-SIMILAR FRONT FORMATION

It is natural to ask if the evolution of the front is asymptotically self-similar. Figure 3 is a first indication of local self-similarity during front formation. This as well as the following analysis is done for the standard initial condition (3). The scenario is meant locally. For the initial conditions studied here the symmetrically arranged steepest points move towards the point (π,π). This point conveniently defines our $r=0$. For the entire subsequent analysis the saddle at (π,π) is used rather than the equivalent one at $(0,0)$. The major conclusions of this section are (a) the center has constant Gaussian curvature, and (b) the front undergoes a (generalized) self-similar evolution (c) of such a simple form that finite-time blowup is impossible.

A. Evolution of hyperbolic saddle

Figure 4 shows several time shots of the contour lines in the neighborhood of the center point. The initial condition has a hyperbolic saddle in the center that evolves into a long almost parallel ridge at late times.

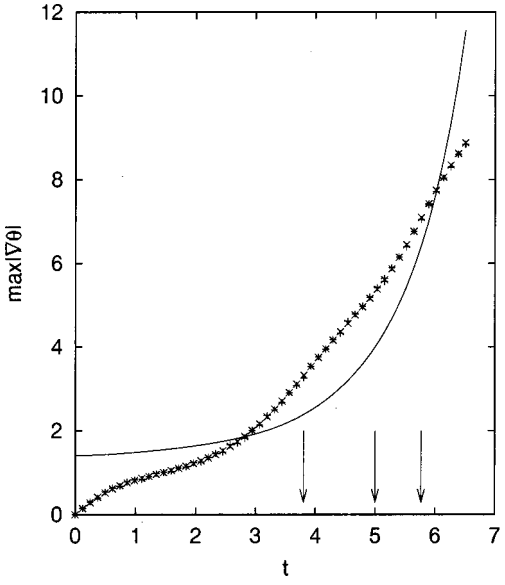

FIG. 2. The maximum gradient (solid line) is rapidly growing. The dots $(+,\times)$ are the stretch rate at the maximum gradient calculated in two different ways from the same pseudospectral simulation and multiplied by 10 for better visibility. The arrows indicate a change in grid resolution (512^2–4096^2).

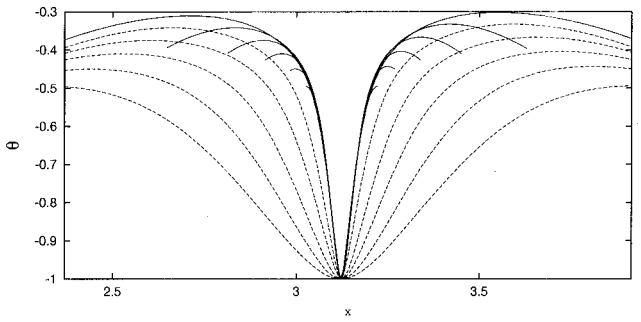

FIG. 3. Self-similarity in a one-dimensional cross section along the x direction. The dashed lines are $\theta(.,\pi;t)$ at different times ($t=4.05, 4.54, 5.03, 5.52, 6.01, 6.50$). The full domain is $2\pi\times 2\pi$. The solid lines are the dashed lines spatially squeezed. They match each other over a wide region, including the steepest points.

To measure the change in geometry we consider the flat center of the hyperbolic saddle. The Gaussian curvature K and the mean curvature H of a surface are given by

$$K=\frac{\theta_{xx}\theta_{yy}-\theta_{xy}^2}{(1+\theta_x^2+\theta_y^2)^2},$$

$$H=\frac{(1+\theta_x^2)\theta_{xx}-2\theta_x\theta_y\theta_{xy}+(1+\theta_y^2)\theta_{yy}}{2(1+\theta_x^2+\theta_y^2)^{3/2}}. \tag{4}$$

The two principal curvatures λ_+ and λ_-, which are the inverse of the two radii of curvature, are obtained from $K=\lambda_+\lambda_-$, $H=\lambda_++\lambda_-$. The angle β of the hyperbolic saddle is determined by $\tan^2(\beta/2)=-\lambda_-/\lambda_+$.

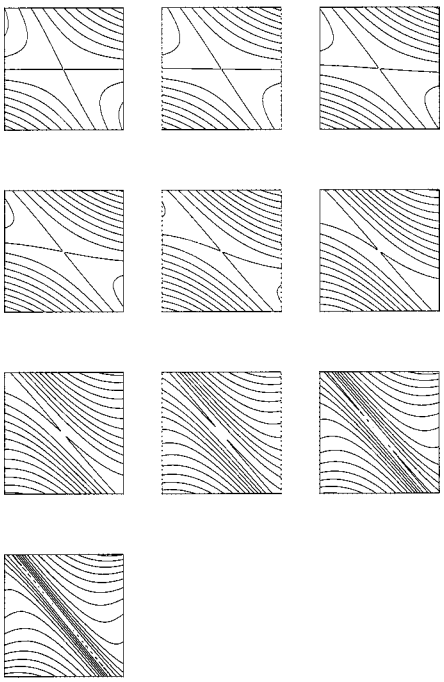

FIG. 4. Contour plots of the neighborhood around the center. The length of the square is $\pi/2$; the entire domain has 2π. The plots are shown in constant intervals of about 0.61 time units ($t=0,0.61,\ldots,5.52$). Two fronts with a hyperbolic saddle in between approach each other. The breakup of the center line is an artifact of the contour plotting algorithm.

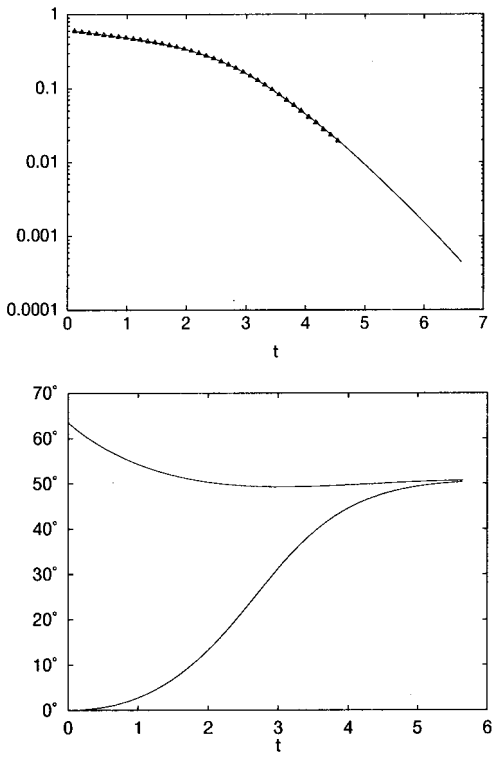

FIG. 5. (a) Curvatures at the center of the domain. The dots (triangles) are λ_-, which suffer from numerical cancellation errors at late times (not plotted). The solid line is $-1/\lambda_+$, which has to be identical to λ_- for all times. Since $\tan(\beta/2)=\lambda_-$ this shows the closing of the saddle angle. (b) The angles of the hyperbolic saddle lines with respect to the x axis. The difference between these two angles is β.

The Gaussian curvature at the center of the domain, or equivalently at (0,0), always remains -1. This can be derived in the following way: θ is symmetric around (0,0), hence $\nabla\theta(0,0;t)=0$ and $v(0,0;t)=0$ for all times. Taking successive spatial derivatives of Eq. (1) yields

$$\partial K/\partial t=-2K\nabla\cdot v=0. \tag{5}$$

This says that there will always remain a hyperbolic saddle at the center. It also connects the two principal curvatures at the center point with each other, so that flattening in one direction corresponds to steepening in the perpendicular direction.

Figure 5(a) shows the two principal curvatures as measured from numerical solutions. When the second derivatives are high K is the difference of two large numbers. Thus, a large numerical cancellation effect occurs in calculating small Gaussian curvatures. Because of this cancellation effect λ_- cannot be measured for long, but λ_+ has no such problem. The two are connected with $K=\lambda_+\lambda_-=-1$. The data in Fig. 5(a) clearly show the flattening of the front in one direction while the curvature in the other direction increases. The saddle angle closes, but never reaches zero.

(Assuming the solution is locally well approximated by a hyperboloid, one can easily convince oneself that there is no

singular motion in the flat direction of the saddle. Suppose we choose the y axis along the ridge. The gradient within the saddle, a small distance y away from the center, will be of order $\theta_{yy}y^2/\beta y \sim -\lambda_- y/\beta \sim \sqrt{-\lambda_-\lambda_+}y = \sqrt{-K}y = y$, which is small. So there are no high gradients formed below the saddle point.)

At late time the gradient growth is dominated by inward moving almost parallel contour lines, not the closing motion of the saddle. The speed of the inward moving parallel contour lines can be measured, for instance, from fits like the one necessary to produce Fig. 3. Unfortunately, the time interval over which this motion occurs in the simulations is too small to allow any reliable asymptotic fit, but the inward velocity certainly increases with time. The two fronts, moving towards each other, squeeze in between them a thin saddle. In between the tiny angle of the saddle there is no notable gradient.

A quantity not captured in curvature measurements is given in Fig. 5(b) in terms of the angle of the two major axes of the hyperbolas with respect to the horizontal axis. Neither of them comes completely to rest. If one of them would come to complete rest and if the relative motion to neighboring contours is not singular then the scenario would be exactly described by a theorem of Cordoba [10]. It will be treated in more detail below. What we observe is a slight variation of this scenario.

B. Self-similarity ansatz

Self-similarity would mean that the solution at a later time can be obtained by spatial rescaling of the solution at an earlier time. For a generalized self-similar scenario we allow a general linear transformation

$$\theta(r;t) = \theta(B(t,t_0)r;t_0). \tag{6}$$

$B(t,t_0)$ is an invertible 2×2 matrix that may blowup in finite time.

The matrix of second derivatives

$$\Lambda = \begin{pmatrix} \theta_{xx} & \theta_{xy} \\ \theta_{yx} & \theta_{yy} \end{pmatrix} \tag{7}$$

at the center point is given by $\Lambda(t) = B^T\Lambda(0)B$, so that the constant Gaussian curvature $\det\Lambda$ enforces $\det B = 1$. The alternative $\det B = -1$ is clearly impossible.

We can obtain a fit for the matrix B from the numerical solution. The details of this fitting procedure can be found in the Appendix. The measured coefficients of B are plotted in Fig. 6. In the first graph $B(t+\Delta t,t)$ is shown in a basis with one axis along the ''final'' orientation of the ridge (fixed in time, orthonormal). There is no indication of such a fixed asymptotic orientation, but it is changing only slowly at late times. The motion is self-similar at the beginning and at late times but the fitting ceases to converge for times around 1.3–2.3, indicating no self-similarity. It is a transition from one kind of self-similarity to another. The determined B is close to the one investigated by Cordoba [10] where

$$B = \begin{pmatrix} b_{11} & b_{12} \\ 0 & b_{22} \end{pmatrix}.$$

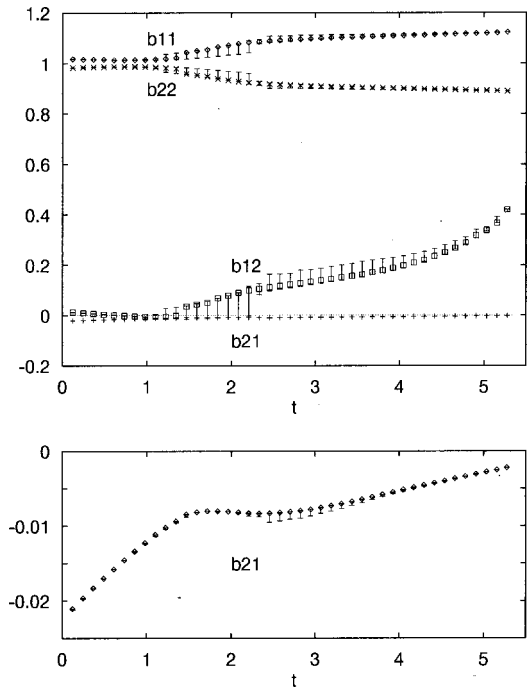

FIG. 6. The four coefficients of the matrix B that describe locally the generalized self-similar motion of the contour. (a) The differential $B(t,t-\Delta t)$ with $\Delta t \approx 0.12$ in a rotated basis. The error bars are from different fit parameters as described in the Appendix. (b) offers an enlarged view of the coefficient b_{21}.

The off-diagonal b_{21}, however, appears to pass asymptotically through zero as is evident from Fig. 6(b).

Unfortunately, the available numerics does not reach far enough in time to reveal the asymptotic form of $B(t,t_0)$, and we will hence not present integration of the data in Fig. 6. At any rate, $\det B = 1$ reduces the number of functions that describe the front motion close to the center from 4 to 3.

C. Comparison with proposed scenarios

For some simple contours θ and time evolutions B it can be proven there is no local singularity in finite time [14]. The exact conditions follow.

(1) There is a nondegenerate critical point, that is, there is an invertible, symmetric matrix Λ such that $\nabla\theta(r;t_0) = \lambda(r,t_0)\Lambda(t_0)r$. ($\Lambda$ is again the matrix of second derivatives at the center.)

(2) $||B||^2 \leqslant C||B^T\Lambda B||$. If this condition is valid the scenario will be called ''proper.''

A proper, nondegenerate generalized self-similar blowup cannot happen in finite time for the active scalar. The maximum gradient is in this case bounded by a double exponential [14].

The first condition is fulfilled because $\det\Lambda = -1$ for all times. For the initial contour

$$\Lambda = \begin{pmatrix} 0 & 1 \\ 1 & 1 \end{pmatrix}.$$

The right hand side of the second condition $C||B^T\Lambda B|| = C||\Lambda(t)||$ and is independent of the reference time t_0. In the supremum norm $||\Lambda(t)|| = |\lambda_+(t)|$. The left hand side of

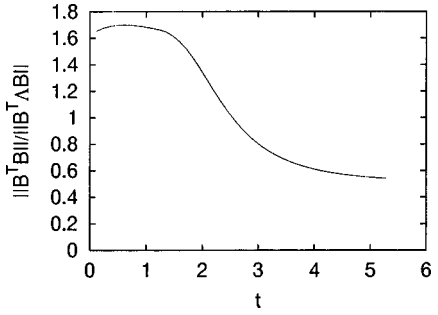

FIG. 7. Direct verification of the ''properness'' of the self-similarity ansatz $||B^TB||/||B^T\Lambda B|| \leq C$.

condition (2) changes under a different choice of t_0 only by a factor. A direct verification of condition (2) (with $t_0=0$) is shown in Fig. 7. The special cancellation necessary to render condition (2) invalid does not happen. The self-similarity ansatz is indeed proper and nondegenerate, that is, the maximum gradient grows (locally) at most like a double exponential. (Here a general constant is allowed in front, unlike the numerical fit proposed for the growth.)

Close to the saddle point, θ is constant along hyperbolas. The coefficients of the hyperbolas are associated with the coefficients of the B matrix. For the scenario treated in [10]

$$C=xy+\frac{a(t)}{2}y^2. \tag{8}$$

An arbitrary smooth rescaling of the x and y axes would be allowed, but this is unnecessary given the Gaussian curvature is -1. The form (8) is preserved under a spatial transformation $r'=Br$ of the form

$$B=\begin{pmatrix} b_{11} & b_{12} \\ 0 & 1/b_{11} \end{pmatrix}.$$

IV. OTHER INITIAL CONDITIONS

All numerical work on singularities in SQG so far [8,3,15,9,7] has dealt with one initial condition (3). In a systematic search for singularities we used a Fourier expansion of the form

$$\theta(x,y;0)=\sum_{m,n=0}^{2}[a_{mn}^{(1)}\sin(mx)\sin(ny) + a_{mn}^{(2)}\sin(mx)\cos(ny)+a_{mn}^{(3)}\cos(mx)\sin(ny) + a_{mn}^{(4)}\cos(mx)\cos(ny)], \tag{9}$$

with 24 independent coefficients as initial data. For some searches many of these coefficients have been set to zero. The others are chosen randomly between -1 and $+1$ (or a smaller interval). Hundreds of initial data are picked and run on a coarse grid. The most promising candidates, judged by whether the maximum gradient seems to exceed a double exponential or not, are picked out and run on a refined grid. A sample collection of some of these promising candidates is shown in Fig. 8. None of the initial conditions tried revealed signs for a finite-time blowup.

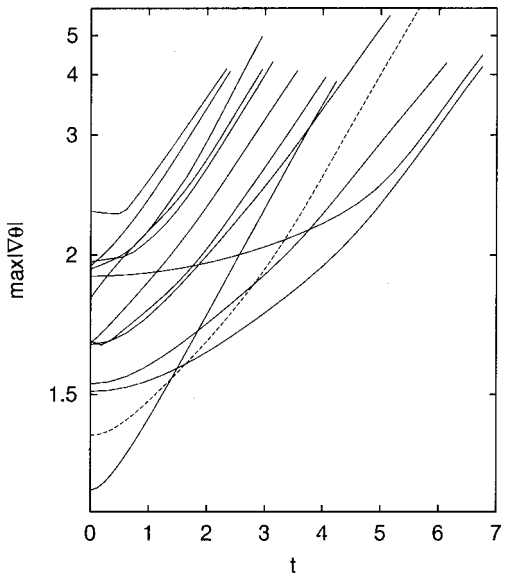

FIG. 8. Some rapidly growing gradients for different initial data. The maximum gradient on the ordinate is plotted on a double logarithmic scale. None, however, seems to evolve faster than a double exponential. The dashed line is for the standard initial condition.

Fronts cause sudden temperature changes and wind jets. It is of geophysical relevance to understand under what conditions particularly steep thermal fronts form. Looking at temperature fields for initial conditions like the ones for Fig. 8 shows that rapid growth is not at all restricted to double fronts around hyperbolic saddles. Single fronts and fronts close to parabolic points are also among them.

V. CONCLUSION

In one numerical solution with rapidly growing gradients the front forms in a generalized self-similar way around a point of constant Gaussian curvature. As a result thereof, the contour motion is locally described by at most three functions of time. A search over other initial data (with periodic boundary conditions) brought no new candidate for singularity formation. Obviously one is led to conjecture that SQG has no finite-time singularities. Approximately double exponential growth is found frequently with various front geometries.

ACKNOWLEDGMENTS

N.S. gratefully acknowledges help by Leo Kadanoff, Norman Lebovitz, and Ray Pierrehumbert. N.S. was partially supported by the ASCI Flash Center at the University of Chicago under U.S. DOE Contract No. B341495. P.C. was partially supported by NSF Grant No. DMS-980-2611 and the DOE-ASCI Center at the University of Chicago. Q.N. was partially supported by the Accelerated Strategic Computing Initiative Center (DOE) and Materials Research Center (NSF) at the University of Chicago.

APPENDIX: NUMERICAL FIT FOR SELF-SIMILARITY ANSATZ

We can obtain a fit for the matrix B by matching θ at a given time t to a spatially distorted θ at a later time, $\theta(r;t+\Delta t)=\theta(B(t+\Delta t,t)r;t)$. The fitting is done by minimizing $\Sigma_{x,y}|\theta(x,y;t+\Delta t)-\theta(B(x,y);t)|w(x,y)$ as a function of the four matrix elements of B. The weighting function w is chosen to decay away from zero like $w(r)=W/|r|-1$. W is the maximum width of the domain considered for fitting (say $W\approx 0.3$). w is set to zero when $\theta(x,y)>-0.65$ (the center point is at $\theta=-1$). Interpolation of the distorted grid back to the uniform grid is done by bilinear interpolation [16].

The errors in this fitting are about the same as fitting the contour to itself after a back and forth transformation. This evidence for self-similarity is complemented by visual checks of the transformation.

If the motion is locally self-similar B also retrieves the second derivatives at the center point, which serves as additional check on the numerics. Also the constraint $\det B=1$ can be applied to replace one coefficient. Larger time intervals Δt have to leave the integrated result unchanged. For the error bars in Fig. 6 the following variations are undertaken: $W=0.2$, 0.3, 0.4, the weighting function to the first and 3/2 power, cutoff of θ at -0.65 and -0.7. The determinant constraint has been used to replace the first coefficient. This replacement reduces the error bars at late times.

[1] J. Pedlosky, J. Atmos. Sci. **21**, 201 (1964).

[2] J. Pedlosky, *Geophysical Fluid Dynamics*, 2nd ed. (Springer, New York, 1987).

[3] P. Constantin, A. Majda, and E. Tabak, Nonlinearity **7**, 1495 (1994).

[4] T. Dombret, A. Pumir, and E. Siggia, Physica D **57**, 311 (1992).

[5] I. Held, R. Pierrehumbert, S. Garner, and K. Swanson, J. Fluid Mech. **282**, 1 (1995).

[6] P. Constantin, SIAM (Soc. Ind. Appl. Math.) Rev. **36**, 73 (1994).

[7] P. Constantin, Q. Nie, and N. Schörghofer, Phys. Lett. A **241**, 168 (1998).

[8] P. Constantin, A. Majda, and E. Tabak, Phys. Fluids **6**, 9 (1994).

[9] K. Ohkitani and M. Yamada, Phys. Fluids **9**, 876 (1997).

[10] D. Cordoba, Proc. Natl. Acad. Sci. USA **94**, 12769 (1997).

[11] N. Schörghofer, Ph.D. thesis, University of Chicago, 1998 (unpublished).

[12] C. Canuto, M. Y. Hussaini, A. Quarteroni, and T. A. Zang, *Spectral Methods in Fluid Dynamics* (Springer, New York, 1988).

[13] There are known examples in fluid mechanics for which a double exponential has been proven as an upper bound on the maximum gradient [17].

[14] P. Constantin, J. Stat. Phys. **93**, 717 (1998).

[15] A. Majda and E. Tabak, Physica D **98**, 515 (1996).

[16] W. Press, S. Teukolsky, W. Vetterling, and B. Flannery, *Numerical Recipes in Fortran*, 2nd ed. (Cambridge University Press, Cambridge, England, 1992).

[17] A. Bertozzi and P. Constantin, Commun. Math. Phys. **152**, 19 (1993).